Defrost Smarter: Compact TES for HVAC Peak Load Reduction

Sven Mumme and Wyatt Merrill, U.S. Department of Energy
Jason Woods, Conrado Ermel, Thomas Freeman, National Laboratory of the Rockies
Kyle Gluesenkamp, Bo Shen, William Doktycz, Navin Kumar, Oak Ridge National Laboratory
Samuel Rosenberg, Pacific Northwest National Laboratory

ABSTRACT

Peak electricity demand—not average energy use—drives grid size and costs. Buildings, particularly HVAC systems during extreme weather, set much of that peak. Full-scale thermal energy storage (TES) can help – but its multi-hour capacity, high cost, complex controls, and space needs limit adoption. TES for defrost, by contrast, requires just 10 minutes of storage per hour, which demands higher power density but enables a smaller footprint, simpler integration, and lower cost – while directly addressing "cold blow," a major consumer complaint during defrost.

This paper analyzes two approaches for TES-enhanced defrost for air-sourced heat pumps. Both approaches were developed as laboratory scale systems and experimentally tested to evaluate their performance. The experimental results were subsequently used to calibrate the equipment model and inform building-level simulations. The first is a small TES housed inside the outdoor unit, interfacing with the refrigerant through a TES-refrigerant heat exchanger, which enables the indoor air circulation to be turned off during defrost. The second is a phase change materials (PCM) module integrated in the supply air duct, allowing heat exchange between PCM and supply air, which enables continuous heating to the building during defrost.

The paper will quantify projected regional benefits, showing how TES-based defrost can reduce energy use, shave peak demand, and lower grid capacity requirements – delivering value for both consumers and the electricity system – while offering a practical, cost-effective, near-market-ready solution poised for immediate impact.

Introduction

Performance, grid impacts, and cost: a primer on the challenges of business-as-usual HVAC defrost

Air-source heat pumps operating in heating mode must periodically enter defrost to remove frost accumulation from the outdoor coil. Frost forms when humid air contacts a coil surface operating below freezing. Because the outdoor coil functions as the evaporator during heating operation, it must remain cold enough to extract heat from ambient air, and frost formation under certain conditions is unavoidable.

Defrost is typically initiated using time-temperature logic or inferred performance degradation rather than direct frost measurement. When a defrost cycle is triggered, two things generally occur. First, the refrigeration cycle reverses, sending hot refrigerant to the outdoor coil to melt accumulated frost. Second, auxiliary electric resistance (ER) heat is activated to offset the temporary cooling effect indoors. While effective at removing frost, this sequence carries penalties that extend beyond the defrost interval itself, leading to cascading negative impacts on unit performance, occupant comfort, and, in aggregate, the electrical grid.

Reverse-cycle operation temporarily interrupts space heating while continuing to consume compressor power, reducing effective system efficiency. Engagement of ER auxiliary heat—typically with a coefficient of performance near unity—further degrades overall performance. Even when auxiliary heat is active, occupants often experience reduced supply air temperatures, commonly referred to as “cold blow.”

The electrical implications of defrost are more pronounced. A representative 3–4 ton residential heat pump may draw approximately 2–4 kW during steady heating operation. During defrost, simultaneous compressor operation and 5–10 kW of auxiliary heat can increase instantaneous demand to 7–14 kW. In many systems, this becomes the highest electrical demand condition experienced throughout the year.

Although individual defrost events are brief, infrastructure must be sized for peak load, not average consumption. As a result, short-duration auxiliary heating events can influence service panel sizing, distribution transformer loading, and feeder capacity. The effect becomes more significant when considered in aggregate, though decision makers are expected to consider both the costs and benefits of mitigating synchronized, aggregated defrost power peaks, including their estimates of the frequency of such events.

Frost formation is most common when outdoor temperatures are near the freezing point and humidity is elevated, conditions typical during winter precipitation events and frontal passages. During these periods, heating loads are already high, and compressors operate for extended durations, accelerating frost accumulation. This phenomenon is particularly exacerbated in certain regions, specifically those with a relatively large number of humid days between 30°F and 45°F (approximately -1°C to 7°C). Because many residential systems rely on similar time-based or temperature-based defrost initiation logic, and because frosting conditions often persist for hours, units exposed to the same weather conditions tend to enter defrost within overlapping intervals.

A weather-weighted assessment suggests that approximately 20–30% of installed heat pumps may be in defrost simultaneously during sustained frosting events (Li et al. 2024, Milev et al. 2023, NEEP 2024). For a region with 1 million operating heat pumps, a 25% coincidence rate corresponds to roughly 250,000 units defrosting within overlapping time windows. If each unit experiences an incremental 5 kW increase above steady heating demand, the coincident load increase approaches 1.25 GW. This clustering occurs during periods when heating demand is already elevated, sharpening winter peak demand rather than occurring independently of it. In retrofit applications constrained by 100-A service limits, defrost-related peaks can influence panel upgrade requirements. At larger scales, coincident defrost auxiliary heating contributes to transformer loading and feeder capacity considerations. Ultimately, these infrastructure requirements are reflected in system costs.

Despite its frequency and electrical intensity, defrost control remains largely unchanged across residential systems. Most equipment infers frost rather than measuring it directly and relies on fixed or semi-fixed initiation intervals. Once initiated, little effort is made to reduce the electrical intensity of the defrost event itself. This creates an opportunity to target the peak component of defrost without altering the broader heating system architecture.

Alternative approach: thermal energy storage for defrost

Rather than attempting to perfect defrost timing through additional sensing and control complexity, a more practical approach is to reduce the electrical intensity of the defrost event itself. A small amount of thermal energy storage (TES)—sized only to bridge the defrost interval—can be integrated with relatively low cost and system complexity while addressing the primary performance and peak-demand penalties associated with reverse-cycle operation.

Full-scale TES applications in buildings, such as chilled water and ice storage tanks, are already used to manage peak demand and shift multi-hour loads. However, their large capacity requirements, cost, and space constraints limit adoption primarily to larger facilities. Defrost-specific TES presents a fundamentally different design problem. Instead of shifting hours of load, the objective is to supply heat during a short-duration event—typically on the order of 10 minutes per hour under sustained frosting conditions. This requires comparatively high discharge power but modest total energy capacity, enabling compact form factors and simplified integration within residential HVAC equipment.

The operational principle of TES-assisted defrost is straightforward: thermal energy is stored during normal heating operation and discharged during defrost through a heat exchanger (HX), reducing or eliminating the need for auxiliary ER heat. Depending on configuration, stored heat may be delivered directly to the refrigerant circuit or to the indoor air stream.

Multiple engineering pathways exist for implementing TES-assisted defrost (Shen et al. 2018). Storage media may be sensible (utilizing specific heat) or latent (utilizing phase change material, PCM). Integration may occur on the refrigerant side—providing a higher-temperature heat source for evaporation during defrost—or on the air side, supplying heat to the delivered air stream. Each pathway carries implications for system configuration, control strategy, packaging, and heat exchanger design.

Device performance during defrost depends not only on nominal energy capacity but also on discharge power capability. Devices with similar stored energy can exhibit substantially different power delivery depending on heat exchanger geometry and internal thermal transport limitations (Woods et al. 2021). Key parameters include TES thermal conductivity, PCM thickness, fluid channel spacing, flow rate, and thermal contact resistance between the TES and the HX channel walls. Enhancing PCM conductivity through fillers may improve power delivery but typically reduces total storage capacity, creating tradeoffs between energy, power, cost, and manufacturability. Consequently, two TES devices with similar apparent performance may differ meaningfully in cost and integration complexity.

This paper evaluates two TES-assisted defrost configurations reflecting these design pathways. Both configurations are prototype systems developed for research and optimization of the configuration and are not currently commercially available. The first integrates a compact TES module within the outdoor unit, interfacing with the refrigerant circuit. The second integrates a PCM module within the supply air duct, delivering heat directly to the indoor air stream during defrost. Experimental results from laboratory scale testing for each configuration were subsequently used to inform, building-level and regional modeling to quantify impacts on energy performance, individual building peak demand, and aggregated winter peak demand across representative U.S. regions.

Approach

Two TES-enhanced system configurations were considered, as shown in Figure 1, prototype, and a model was developed for each equipment configuration type. In addition, a representative building model based on the 5RC1 resistance-capacitance circuit analogy presented by EN ISO 13790 was used for each region. Both TES-enhanced prototypes have been tested in the laboratory but are not commercially available or have been tested in the field. For the refrigerant-based TES integration configuration, laboratory testing results were used to calibrate the model for pump power, building heating capacity, TES charging capacity, and cooling capacity during defrost operation for both the baseline system and the TES-integrated prototype based on 3-ton heat pump. For the air-based TES integration configuration, a prototype of the TES was tested using emulated supply air temperatures during both heating and reverse-cycle defrost modes. This test data was used to calculate the outlet air temperature in the building simulations. Then, each equipment type was modeled in each region, and the results were scaled to predict the impact on heating energy consumption and peak demand reduction across the regions. Each of the sub-models and the approach to aggregation is described in the following sections.

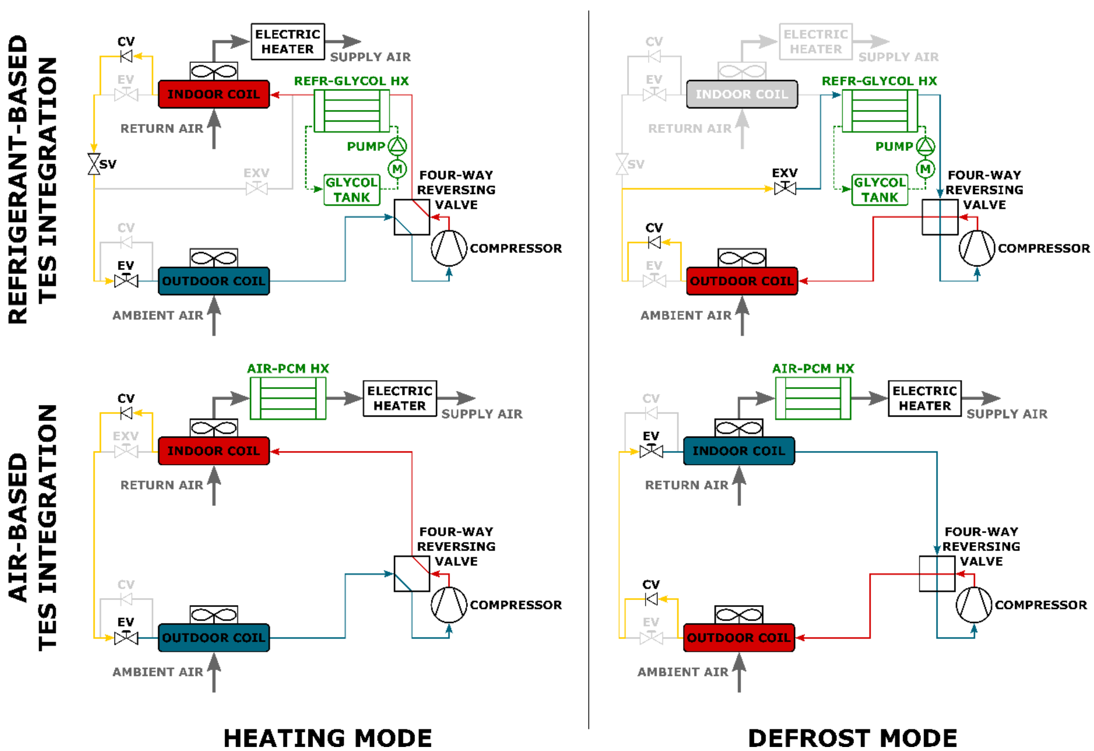

Figure 1: Two methods for integrating TES into a heat pump to support defrost. Top: Integration into the refrigerant circuit. Bottom: Integration into supply air.

A summary table comparing the two TES-enhanced configurations, and their respective baseline systems, is shown in Table 1. Each TES-enhanced system required its own baseline, since the air-based configuration used a variable speed compressor (sized for heating load) and variable capacity ER; while the refrigerant-based configuration used a single speed compressor (sized for cooling load) and fixed capacity ER. There is nothing to prevent either configuration working with variable or single speed systems, and this is left for future work.

Table 1. Comparison of the four systems considered in this work

	Air-based configuration		*Refrigerant-based configuration*	
	Baseline	*TES*	*Baseline*	*TES*
Defrost initiation criterion	60 min cumulative run time below 40°F ambient dry bulb*, adjusted for PLR		60 min cumulative run time below 40°F ambient dry bulb*	
Defrost duration (termination)	1-6 minutes, depending on ambient condition (see Table 4)			
Defrost method	Reverse cycle. Indoor air as heat source.	Reverse cycle. Indoor air as heat source, PCM in duct	Reverse cycle. Indoor air as heat source.	Reverse cycle. TES as heat source.
Electric resistance (ER) usage during defrost	On; varied to meet building load	On; varied to meet rest of building load	On (single stage)	None
HVAC system type	Variable speed compressor		Single speed compressor	
System sizing	sized for heating load at 10°F		sized for cooling load	
Balance point†	10°F ambient		~25°F ambient	
Auxiliary ER heat usage to meet building setpoint	Variable capacity, controlled as needed to meet building setpoint below balance point		On/off control, 7–15 kW depending on region, turned on as needed to meet setpoint below balance point	
Assumed lowest ambient temp for compressor operation	0°F			

*the timer for cumulative run time resets when the ambient rises to 52°F
†the balance point is the ambient temperature above at which the compressor can just meet the entire building load

Our simulations focus on a typical single-family residential building in the United States, with a floor area of 2150 ft^2. Our building model is a 5R1C model, which has been verified with output from the OCHRE simulation engine (NLR 2026).

Our simulations span regions 3 to 7 in the US, including humid (A) and dry (B) regions. We use the Typical Meteorological Year (TMY) weather for one city for each region, with the representative city based on those used for the DOE reference buildings (DOE 2013). TMY files are created to represent typical hourly weather for different locations (Wilcox et al. 2008).

Equipment model: defrost duration

The duration of defrost events was characterized using the segment-by-segment heat exchanger frost and defrost models in DOE/ORNL Heat Pump Design Model (HPDM) via quasi-steady-state system simulation. A 4-ton, two-stage Goodman heat pump using R-32 was modeled. The simulation predicts frost formation over 60 minutes with an indoor airflow rate of 1,200 CFM and an outdoor airflow rate of 3,200 CFM; the compressor operates at full capacity during both frosting and defrost. During defrost, the outdoor fan is off, while the indoor fan maintains 1,200 CFM to enable heat absorption from the indoor air.

Table 2 summarizes the simulated frost mass accumulated on the outdoor coil after one hour as ambient temperature varies from 40°F to 10°F and outdoor relative humidity from 90% to 35%. The results indicate that the frost formation rate decreases as ambient temperature and outdoor relative humidity decrease.

Table 2. Frost accumulation for baseline system

frost mass [kg]		RH				
		0.9	0.8	0.7	0.6	0.35
Tamb °F	40	4.81	2.95	1.20	0.00	0.00
	30	3.07	1.87	0.76	0.00	0.00
	20	1.75	0.92	0.27	0.00	0.00
	10	1.01	0.48	0.04	0.00	0.00

Table 3 shows the modeled system COP with a frost-free coil and the degradation ratio experienced by the system after 60 minutes of frosting. It was assumed that all moisture condensed on the outdoor coil froze instantaneously, adding thermal resistance to the tube and fin surfaces.

Table 3. COP of clean coil (free of frost) and COP degradation ratio after 60 minutes of frosting

COP		RH									
		0.90		0.80		0.70		0.60		0.35	
		clean	frosted	clean	frosted	clean	frosted	clean	frosted	clean	frosted
Tamb °F	40	3.44	0.99	3.41	0.99	3.38	0.99	3.35	1.00	3.35	1.00
	30	3.12	0.90	3.09	0.94	3.07	0.97	3.05	1.00	3.05	1.00
	20	2.76	0.77	2.74	0.85	2.73	0.95	2.72	1.00	2.73	1.00
	10	2.41	0.74	2.41	0.86	2.40	0.99	2.40	1.00	2.40	1.00

To compute the defrost duration (from defrost initialization to defrost termination) at each ambient condition, HPDM initialized the defrost mode with the frost mass accumulated after 60 minutes of operation at that ambient condition. The coil surface temperature distribution at the end of the one-hour frosting period was used as the initial condition for defrost.

The defrost energy balance included the latent heat required for melting the accumulated ice, evaporating some of the meltwater, the sensible heating of the thermal mass (coils, fins, and frost), and heat losses to the ambient. The fraction of coil heat lost to the surrounding air was assumed to vary linearly with ambient temperature, from 22% at 40°F to 32% at 10°F. This linear relationship was adopted as a first-order approximation-based compressor heat loss as a function of the ambient temperature. This assumption was necessary due to the lack of detailed experimentally calibrated data for the present study.

Defrost was simulated in 10-second time steps, with the outdoor coil and accumulated ice mass divided into ten control volumes (nodes). The defrost simulation continued until the outdoor coil leaving-tube surface temperature (lowest surface temperature) reached 70°F. The defrost process for each node comprised three stages: (1) warming from the post-frost surface temperature to the melting point at 32°F; (2) isothermal melting at 32°F and evaporating a fraction of the meltwater within each control volume; and (3) post-melt sensible heating of the coil metal after frost removal. This spatial discretization allows the model to track local temperature evolution, phase change, and frost removal dynamics across the coil during defrost, with the overall conclusion derived from the aggregate response of all nodes over time. The ratio of meltwater evaporated was treated as a calibrated parameter, obtained by calibrating the simulated defrost time at 20°F and 90% outdoor relative humidity to match an experimentally recorded duration of 230 seconds under those ambient conditions.

Figure 2 illustrates the evolution of surface nodal temperatures during a defrost cycle simulated at an ambient temperature of 20°F and relative humidity of 90%. Defrost heating begins from the coil's metal temperature at the end of the preceding frost-formation cycle. Upon reaching the frost melting point, approximately 80% of the meltwater drains away while 20% evaporates on the surface. After all frost has melted and the residual water has evaporated, the coil surface temperature rises until the defrost cycle terminates when the exit-node temperature reaches 70°F. The discretized coil model indicates non-uniform heating across the coil and pinpoints the node whose temperature triggers defrost termination.

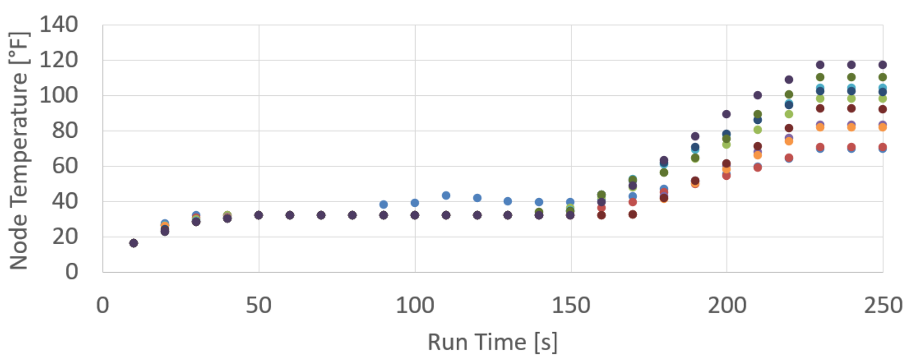

Figure 2. Outdoor coil surface temperatures of the ten modeled nodes during defrost.

The resulting effective defrost duration (s) is reported in Table 4. It includes the time required to remove frost and to raise the coil surface temperature from its initial value to 70°F at the tube section leaving the outdoor coil. Note that this effective defrost duration excludes the refrigerant charge migration period (up to 2 minutes), during which no heat is assumed to be added to the outdoor coil. In the annual cycle simulations implemented in this work, these defrost durations were rounded to the nearest minute. Higher ambient temperatures combined with high relative humidity can increase the absolute moisture content of the air, which promotes faster frost accumulation on the outdoor heat exchanger for a fixed heating duration therefore undergo defrost for longer periods. Whereas at lower relative humidity the defrost duration remains comparatively small and nearly independent of outdoor ambient temperature.

Table 4. Defrost duration for baseline system

defrost duration [s]		RH				
		0.9	0.8	0.7	0.6	0.35
Tamb °F	40	380	360	140	60	60
	30	340	220	120	70	70
	20	230	150	100	80	80
	10	170	170	170	170	170

As indicated previously in comparison Table 1, the defrost durations of Table 4 were used for the baseline systems and the air-based TES-enhanced system. For the refrigerant-based TES-enhanced system, the duration of defrost was shortened. Higher ambient temperatures combined with high relative humidity can increase the absolute moisture content of the air, which promotes faster frost accumulation on the outdoor heat exchanger for a fixed heating duration therefore undergo defrost for longer periods. Whereas at lower relative humidity the defrost duration remains comparatively small and nearly independent of outdoor ambient temperature.

Equipment model: air-based system integration of TES

One option for integrating TES into the heat pump is to directly reheat the air that is cooled during the reverse cycle defrost, as shown at the bottom of Figure 1. The TES is charged (PCM melted) using the hot air exiting the condenser, and then the TES is discharged (PCM frozen) during the defrost period. This requires ~1.5°C higher condensing temperature than the baseline during normal heating operation, so that the same temperature is delivered to the building.

Figure 3 shows test data on an initial prototype using 250 cfm (~1/5 scale), with some PCM panels pulled out for illustration purposes only. The prototype, shown in a photo, consists of 5-mm thick PCM panels encapsulated in aluminum shells separated with 5-mm air gaps. We tested this prototype by controlling the inlet air temperature to emulate heat pump operation with 38°C air temperature during heating mode, and a decaying temperature to 7°C during defrost. The slow change in temperature during defrost is based on testing of a heat pump without TES.

Three representative charge/discharge cycles are shown in Figure 3, starting with a 5-minute defrost cycle. This is followed by a 60-minute heating period, with the 38°C air melting the 35°C transition-temperature PCM. After melting the PCM, the air is still delivered above the target supply-air temperature of 35°C. During the 5-minute defrost cycles, the temperature leaving the indoor coil drops to 7°C, but the TES heats this air back to a more comfortable temperature between 24°C and 30°C. For shorter defrost periods, the delivered temperature will remain at the high end of this range.

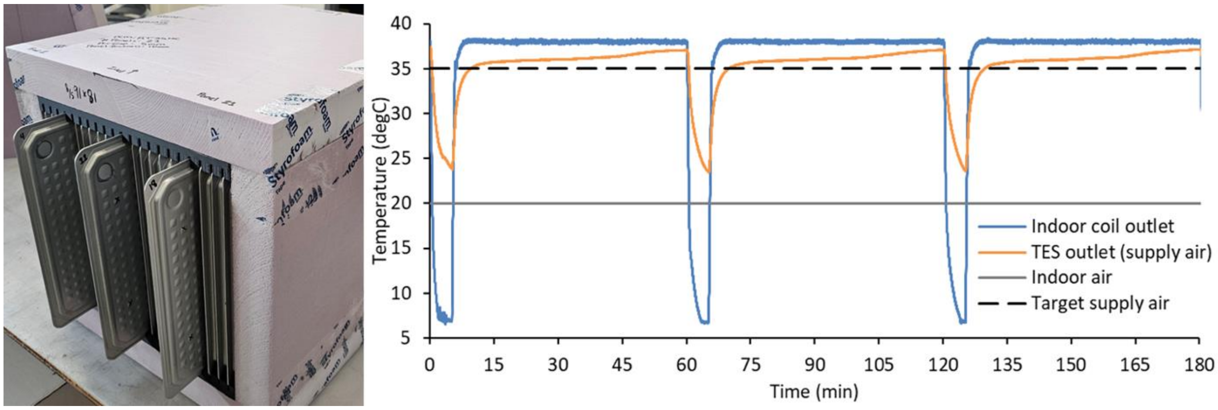

Figure 3: Air-to-PCM heat exchanger prototype (left) and measured data for three defrost/frost cycles (right). Prototype dimensions without insulation are 311 mm (W) x 280 mm (H) x 457 mm (L).

For the simulations, we compare the baseline heat pump to a heat pump that integrates a TES similar to that shown in Figure 3, but sized for a heat pump with a capacity of ~10 kW. The measured pressure drop of 15 Pa at the nominal airflow is adopted for all flow rates in the simulation, which is conservative since pressure drop will be lower as flow is reduced at part load conditions. The indoor fan is assumed to have a constant efficiency of 45%. We assume the TES is sized to counteract all the cooling done during defrost and then provides 35% of the nominal heat pump capacity during that timestep, which is what the prototype did for each 5-minute defrost duration above. If the heating provided is less than the load during defrost, then we assume the backup heater meets the remaining building load during defrost.

Equipment model: refrigerant-based integration of TES

Another option for integrating TES, either sensible or latent, into the heat pump is to incorporate it directly into the refrigerant loop. In this configuration, the TES is charged during normal heating operation, with less than 20 percent of the condenser heating capacity diverted to the TES through a desuperheater or by utilizing a portion of the condensing heat, while the remaining capacity is delivered to the conditioned space. The TES is charged through a secondary hydronic loop, after which the condensing heat bypasses the TES module and is fully delivered to the conditioned space. During defrost operation in cooling mode, the TES is discharged through the secondary hydronic loop to heat the refrigerant on the evaporator side to assist to melt frost on the outdoor coil.

The system was experimentally evaluated at 35°F and 50% relative humidity and 15°F and 75% relative humidity, as summarized in Table 5, using a one-hour operating cycle with a 2–3 minute defrost duration.

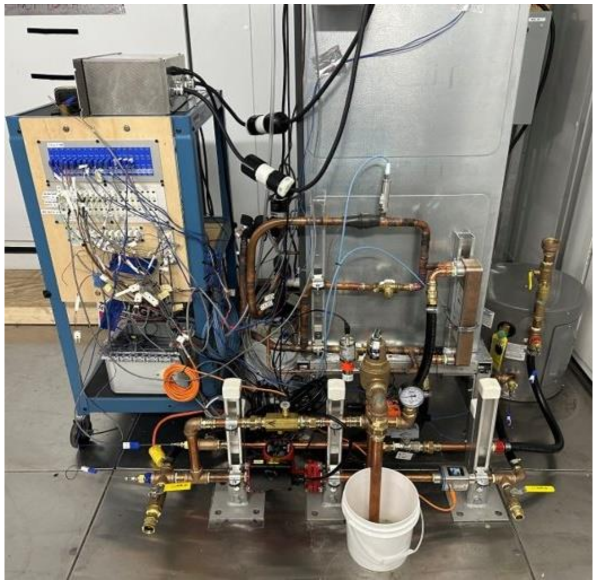

Figure 4. Refrigerant-based Integrated TES Defrost Prototype at ORNL with secondary-loop configuration (Refrigerant/Water Loop) integrated with a heat pump and a 6-gallon sensible storage tank.

Table 5. Electric energy intensity comparison for baseline and TES-based defrost strategies at 35°F and 15°F outdoor temperatures.

Outdoor Temperature (°F)	Baseline w/o Electric Resistance ($Wh_{electric}/kBTU_{th}$)	Baseline with Electric Resistance ($Wh_{electric}/kBTU_{th}$)	Refrigerant-based Integrated TES Defrost ($Wh_{electric}/kBTU_{th}$)
35	1.73	7.8	1.29
15	4.4	6.3	1.5

Building envelope modeling approach – Individual building

The thermal behavior of the 2150 ft^2 dwelling was modeled using the resistance-capacitance circuit analogy presented by EN ISO 13790. The following values were adopted for the respective conductance (1/R) of five resistances and one capacitor (5R1C): air-indoor surfaces $H_{tr,is}$ = 1800 W/K, indoor surfaces-mass $H_{tr,ms}$ = 1200 W/K, building mass-outside (opaque envelope) $H_{tr,em}$ = 100 W/K, indoor surfaces-outside (windows) $H_{tr,w}$ = 60 W/K, and ventilation H_{ven} = 80 W/K. The building's thermal inertia is represented by the capacitor which is assumed to be $C_m = 3x10^6$ J/K. The implementation of the 5R1C model adopted in this work was based on the Python library available in (Ermel et al. 2024).

Equipment modeling approach – Refrigerant-based integration of TES

In the simulation, the performance of a baseline heat pump is compared with that of a heat pump integrated with thermal energy storage (TES), configured as shown in Figure 4. The heat pump, a single-speed minimum efficiency equipment (14.3 SSER2/ 7.5 HSPF2), is sized based on the regional conditions and the peak building cooling load. The thermal energy storage consists of a 10-gallon hot water storage tank filled with a 20 wt% propylene glycol/water mixture. The tank set-point temperature was 90°F, and the stored thermal energy is used to support defrost operation.

For both the baseline and TES-integrated heat pumps, ER heating supplements the heat pump for space heating when the outdoor temperature falls below 25°F. During defrost operation, the ER heater in the baseline mode is activated to maintain an adequate supply air temperature. In contrast, for the heat pump integrated with TES, ER heating is not used during defrost operation.

The defrost counter initiates when the outdoor temperature is below 40°F while the heat pump is operating, and it resets when the outdoor temperature rises above 52°F. In both systems, defrost occurs after every one hour of heat pump runtime when the outdoor temperature is below 40°F.

Auxiliary power assumptions are also included in the simulation. In the baseline, the indoor blower operates during both space heating and defrost operation at a fixed power input of 150 W/ton. For the TES-integrated heat pump, the indoor fan consumes 150 W/ton during space heating and TES charging operation, with an additional pump power of 21.7 W/ton required until the storage tank reaches its setpoint temperature. During TES discharge for defrost operation, the indoor fan remains off, and only the pump power of 21.7 W/ton is considered.

Regional impact modeling approach

We estimate the impacts of TES-assisted defrost in aggregate by scaling results from individual buildings to regions of interest. The number of single-family homes within a region weights the energy savings we calculate for relevant heating modes. Regional calculations assume a simple scaling based on housing unit count from the RECS 2020 Metadata publication (EIA 2022) and the individual-building modeling results, implying homogeneous building characteristics and operational modes. This provides an upper bound on peak load experienced regionally by the grid due to defrost.

Results and Discussion

Individual buildings results – refrigerant-based integration of TES

Table 6 summarizes annual heating simulation results for each region with a single-speed heat pump sized for peak cooling load, comparing cases with and without refrigerant-based TES. The integrated TES modestly reduces annual heating energy use across all regions, with savings of 2.1%–3.9%, while maintaining occupant comfort without relying on electric resistance heating during defrost. Absolute energy savings are higher in colder regions, reaching 381 kWh/year in Duluth, MN. The 15-minute average peak demand reductions are highly variable, ranging from 3% to 60%, and depend strongly on equipment sizing relative to the heating load. In warmer regions like Las Vegas, NV, and Albuquerque, NM, a heat pump sized for cooling is sufficient to meet nearly all winter heating demand, with electric resistance only needed during defrost, resulting in large reductions in winter peak load. In colder regions, heat pumps sized for cooling trigger more frequent electric resistance operation during heating, which reduces the relative impact of TES on peak demand.

Table 6: Energy use and peak demand during defrost for refrigerant-based integrated TES

Location	Region	Annual heating energy use (kWh/y)				Peak heating demand (kW)			
		Baseline	TES	Savings	% savings	Baseline	TES	Savings	% savings
Atlanta	3A	2938	2843	95	3.2%	14.7	2.88	11.8	80.4
Las Vegas	3B	2032	1990	41.7	2.1%	14.4	3.6	10.8	75.0
Baltimore	4A	5351	5143	209	3.9%	14.7	2.8	11.9	80.9
Albuquerque	4B	4369	4204	164	3.8%	14.7	2.9	11.8	80.3
Seattle	4C	3394	3278	115	3.4%	8.4	1.9	6.5	77.3
Chicago	5A	8446	8132	314	3.7%	13.1	2.9	10.2	77.9
Boulder	5B	6025	5877	175	2.9%	10.9	1.9	9	82.6
Minneapolis	6A	12890	12509	381	3.0%	13.1	2.9	10.2	77.9
Helena	6B	8820	8574	246	2.8%	11.1	2.9	8.2	73.9
Duluth	7	13271	12889	381	2.9%	14.2	3.9	10.2	72.5

The defrost performance of single-speed heat pumps with refrigerant-based TES is summarized in Table 7. Across all regions, the TES system substantially reduces defrost energy use, with savings of 74 to 79% compared to the baseline system.

Although the TES configuration results in slightly more defrost cycles with increased heat pump runtime due to charging of thermal storage, which accelerates frost accumulation on the outdoor coil, the defrost energy savings per cycle more than offset the increase in heat pump runtime and the increased defrost cycles; less backup heating is needed during defrost. The largest absolute reductions occur in colder regions, reaching over 1,001 kWh/yr in Duluth, MN, as the number of defrost cycles increases in colder regions that provides more energy saving opportunities with the refrigerant-integrated TES for defrost.

Table 7. Defrost performance summary for refrigeration-based integrated TES

Location	Region	Defrost energy use (kWh/y)				# of defrost cycles	
		Baseline	TES	Savings	% savings	Baseline	TES
Atlanta	3A	245	52.3	193	78.7%	848	876
Las Vegas	3B	94	19	74	79.3%	253	264
Baltimore	4A	561	119	442	78.8%	951	1036
Albuquerque	4B	432	91	341	79.0%	970	1031
Seattle	4C	275	67	208	75.8%	404	453
Chicago	5A	968	220	748	77.3%	1496	1614
Boulder	5B	634	153	481	76.0%	1337	1445
Minneapolis	6A	1233	244	988	80.1%	1820	1943
Helena	6B	913	203	710	78.0%	1818	1966
Duluth	7	1299	297	1001	77.1%	2207	2378

Overall, these results demonstrate that the TES sized and integrated for defrost can significantly reduce both defrost energy consumption and reliance on electric resistance heating, highlighting its potential to improve winter heat pump performance while maintaining comfort, especially in cold regions.

Individual buildings results – variable-speed system with air-based TES

Table 8 summarizes the annual simulation results for each region with the variable-speed system, with and without an air-based TES. In both cases, the system not only offsets the cooling done during defrost but also meets the building load during defrost. Because in some cases the TES does not deliver enough heat to meet the building load, the backup electric heater is still used to ensure the building load is always met, but at a much lower capacity. On average, the additional pressure drops imposed by the TES heat exchanger increased the annual total energy consumption by 1%.

Table 8: Energy use and peak demand for the variable speed system with air-based TES

Location	Region	Annual energy use (kWh/y)				Peak demand (kW)			
		Baseline	TES	Savings	% savings	Baseline	TES	Savings	% savings
Atlanta	3A	3272	3170	101.8	3.1%	17.6	5.2	12.4	70%
Las Vegas	3B	2578	2557	21.0	0.8%	16.1	2.3	13.8	86%
Baltimore	4A	4752	4505	247.9	5.2%	17.9	5.5	12.4	69%
Albuquerque	4B	4255	4086	169.6	4.0%	16.9	3.1	13.8	82%
Seattle	4C	4679	4400	278.6	6.0%	16.5	2.7	13.8	84%
Chicago	5A	6887	6332	554.8	8.1%	18.7	8.5	10.2	55%
Boulder	5B	5908	5540	368.0	6.2%	18.7	8.6	10.2	54%
Minneapolis	6A	8981	8488	493.5	5.5%	18.7	9.9	8.9	47%
Helena	6B	7697	7167	530.2	6.9%	18.8	8.8	10.0	53%
Duluth	7	11622	10871	750.4	6.5%	18.9	9.8	9.1	48%

The energy and demand savings result from the improved performance of the TES system during defrost, which is highlighted in Table 9. Note that there are more defrost cycles for the TES system because of the higher capacity required to charge the TES—higher capacity means more heat is absorbed from outdoors, which means faster buildup of moisture onto the coil as frost. The energy savings per cycle more than compensate for the additional cycles required since the backup heating required is substantially reduced.

Two defrost cycles are illustrated in Figure 5 for the baseline variable speed system for a 6-hour period in January in Chicago. The ambient temperature is around -10°C, and the compressor is modulating down to follow the slowly decreasing building load. The first defrost cycle occurs at minute 155 and lasts for 2 minutes. During this time, the backup electric heater turns on to counteract the cooling during the reverse cycle and to meet the building load. In this case, the electric heater provides 11.5 kW of heat. A similar cycle happens 3 hours later.

Table 9. Defrost performance summary for air-based integrated TES

Location	Region	Defrost energy use (kWh/y)			# of defrost cycles		
		Baseline	TES	Savings	% savings	Baseline	TES
Atlanta	3A	185.4	22.5	163	88%	307	318
Las Vegas	3B	66.9	6.6	60	90%	151	156
Baltimore	4A	412.9	52.4	360	87%	668	690
Albuquerque	4B	314.8	38.7	276	88%	633	654
Seattle	4C	377.5	39.5	338	90%	318	328
Chicago	5A	847.2	119.8	727	86%	1073	1108
Boulder	5B	612.2	89.6	523	85%	918	948
Minneapolis	6A	828.8	133.8	695	84%	1153	1190
Helena	6B	867.2	133.5	734	85%	1223	1262
Duluth	7	1195.7	204.1	992	83%	1353	1395

Figure 5 also shows the same period for the variable speed system with air-based TES. During the 2-minute defrost period, the TES reheats the air, counteracting the reverse cycle cooling and meeting most of the building heating load. To meet the entire building load, the backup element still turns on, delivering just over 2 kW of heat. For the 60-minutes following the defrost cycle, the heat pump provides additional heating capacity to recharge the TES (melt the PCM).

The results in Tables 8 and 9 show that the TES can reduce the heat pump's annual electricity use by ~1-3%, and the peak demand by 40-80%, depending on the region. The larger peak demand savings are seen in the milder regions, where defrost is more likely to be much higher than the peak demand due to the space heating load alone. Because most residential utility rates do not have peak demand charges, it is important to quantify the impact at the local grid scale. This is addressed in the next section.

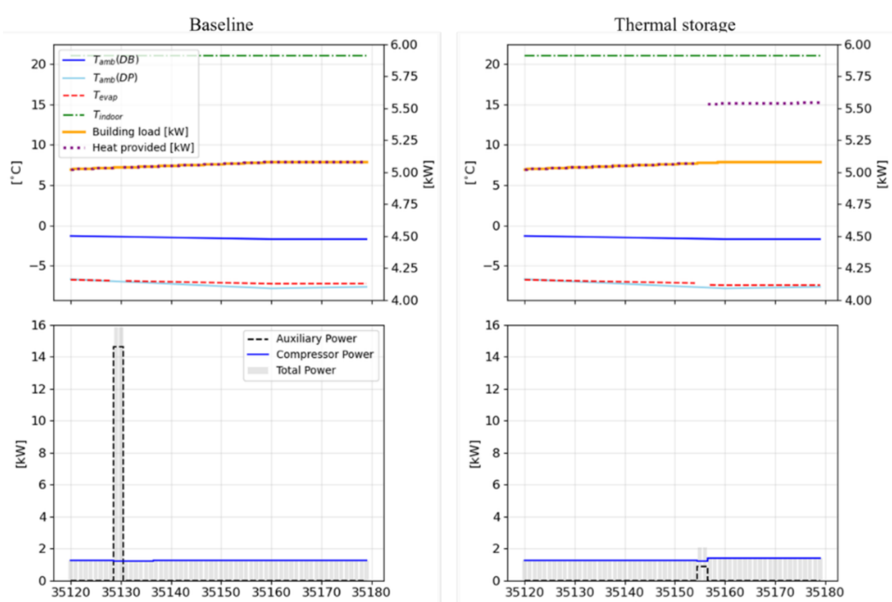

Figure 5. A simulated 6-hour period for a variable speed system in Chicago in January; baseline and air-based TES-enabled.

Regional impact

For the air-based TES configuration, region 5A (cool humid) exhibited the largest potential energy savings at 10,977 GWh/year. For the refrigerant-based TES configuration, region 5A also exhibited the highest energy savings potential at 6,213 GWh/year. The upper bound we calculate on peak demand impacts varied across regions (5.9 to 210.2 GW). Air-based TES produced the greatest reductions in regions 3B (warm dry) and 4C (mixed marine), offsetting 210.2 GW and 201.8 GW, respectively. Refrigerant-based TES achieved the largest peak demand reductions in regions 4A (mixed humid) and 5A (cool humid), each offsetting 201.8 GW. A more accurate approach to calculating peak load impacts would account for the degree to which defrost events occur in coincidence within a given region. Table 10 summarizes the scaled annual heating energy and peak-demand savings for both air and refrigerant-based TES systems across regions.

Table 10. Annual heating energy and peak-demand savings estimated for air- and refrigerant-based TES configurations, scaled to regions sing RECS 2020 single-family housing distributions.

Representative City	**Region**	**Air-based TES**		**Refrigerant-based TES**	
		Yearly heating energy savings (GWh)	Peak demand savings (GW)	Yearly heating energy savings (GWh)	Peak demand savings (GW)
Atlanta	3A	1164	141.8	1086	134.9
Las Vegas	3B	161	105.9	320	82.8
Baltimore	4A	4203	210.2	3543	201.8
Albuquerque	4B	112	9.1	109	7.8
Seattle	4C	699	34.6	289	16.3
Chicago	5A	10977	201.8	6213	201.8
Boulder	5B	1344	37.3	639	32.9
Minneapolis	6A	2689	48.5	2076	55.6
Helena	6B	380	7.2	176	5.9
Duluth	7	576	7.0	292	7.8

Regions 5A, 4A, 6A, 5B, and 3A demonstrate comparatively high annual energy savings potential across both TES configurations. In contrast, regions 4B, 3B, 6B, 7, and 4C show more limited savings potential. For peak demand reductions, the leading regions across configurations include 3B, 4C, 4A, and 5A. These results indicate that annual heating energy impacts are dominated by colder, humid regions with heavy seasonal heating loads, whereas peak demand impacts can be substantial even in milder regions when sharp defrost-related demand spikes are prevalent. We did not model regions 1, 2, and 8.

Discussion

Compact thermal energy storage integrated for defrost support substantially reduced the electrical intensity of heat pump defrost operation while maintaining normal heating performance. Experimental testing and building-level simulations were used to evaluate TES-assisted defrost performance across multiple US regions and system configurations. Prototype testing characterized the behavior of the storage modules during defrost events and verified their ability to deliver short-duration heat at the required defrost power levels. These results informed subsequent simulations using the HPDM, which evaluated annual energy use, peak electrical demand, and heating performance across representative regions.

Across the modeled regions, TES-assisted defrost significantly reduced reliance on electric resistance heating during defrost events. Defrost-specific energy consumption declined by approximately 74–80%, while modeled reductions in 1-minute peak electrical demand ranged from roughly 40–80%, depending on region and system configuration. Annual heating energy use decreased modestly, with reductions of approximately 2–4%.

Peak demand reductions were more pronounced than annual energy impacts because stored thermal energy supplies heat during the brief defrost interval that would otherwise require high-power electric resistance heating. Because defrost cycles tend to occur under similar weather conditions across many systems, reducing the electrical intensity of individual cycles can translate into meaningful reductions in coincident short-duration demand when aggregated across large numbers of heat pumps.

Defrost support also differs fundamentally from conventional thermal storage applications used for load shifting. Traditional thermal storage systems are typically designed to store large amounts of energy for delivery over several hours. In contrast, defrost cycles last only a few minutes and require relatively small amounts of stored energy, but at higher power levels. The results indicate that storage systems designed specifically for this operating regime can remain compact while still substantially reducing the electrical intensity of defrost operation.

Charging the TES modules introduces a modest increase in compressor runtime during normal heating operation. In the modeled cases, this effect was small relative to the reductions in resistance heating and peak electrical demand, indicating that compact TES designed specifically for defrost support can reduce short-duration electrical demand spikes while maintaining heating performance.

Conclusions

This study evaluates compact thermal energy storage approaches designed specifically to support heat pump defrost operation. Experimental testing and building-level simulations demonstrate that TES can reduce the electrical intensity of defrost events while maintaining heating performance during defrost cycles.

The results highlight that defrost support represents a distinct application for thermal storage. Unlike conventional storage systems designed for multi-hour load shifting, defrost operation requires relatively small storage capacity but the ability to deliver heat at high power for short durations. Storage systems designed for this operating regime can therefore remain compact while still mitigating the electrical impacts associated with conventional defrost cycles.

These findings suggest that targeted TES integration may offer a practical pathway for improving heat pump operation during winter conditions while addressing the short-duration electrical demand associated with defrost events.

Acknowledgements

This work was sponsored by the U. S. Department of Energy's Building Technologies Office under Contract No. DE-AC05-00OR22725 with UT-Battelle, LLC, and under Contract No. DE-AC36-08GO28308 with the National Laboratory of the Rockies.

This work is supported in part by Stor4Build, a multi-lab consortium funded by the U.S. Department of Energy (DOE) Building Technologies Office (Awarded Under Lab Call L095). The consortium is co-led by Lawrence Berkeley National Laboratory (LBNL), the National Laboratory of the Rockies (NLR), and Oak Ridge National Laboratory (ORNL). LBNL is managed by the University of California for DOE under Contract No. DE-AC02-05CH11231; NREL is operated for DOE under Contract No. DE-AC36-08GO28308; and ORNL is managed by UT-Battelle LLC for DOE under contract No. DE-AC05-00OR22725.

This research used resources at the Building Technologies Research and Integration Center, a DOE Office of Science User Facility operated by the Oak Ridge National Laboratory.

The authors also acknowledge the contributions to developing the refrigerant-based experimental prototype from Paul Armatis, Xiaobing Liu, Charlie Pierce, Tim Dyer, Brent Massey, and Robert Nettles (ORNL).

References

DOE (U.S. Department of Energy). 2013. "Commercial Reference Buildings." Office of Energy Efficiency & Renewable Energy. https://www.energy.gov/eere/buildings/commercial-reference-buildings.

Dong, J., S. Li, Y. Yao, Y. Jiang, Y. Tian, and H. Tian. 2015. "Defrosting Performances of a Multi-Split Air Source Heat Pump with Phase Change Thermal Storage." *International Journal of Refrigeration* 55: 49–59.

EN ISO 13790, Energy Performance of Buildings - Calculation of Energy Use For Space Heating and Cooling, ISO, Geneva, 2008.

Ermel, Conrado, Marcus V. A. Bianchi, and Paulo S. Schneider. 2024. "Open-Source Simulation Platform for Air Source Heat Pump Integrated with Thermal Energy Storage." *Science and Technology for the Built Environment*, 2024, 30(7), 858–876.

Li, Z.-L., C.-L. Zhang, H.-M. Liu, and X.-C. Wang. 2024. "Feasibility Analysis of Thermal Storage Defrosting Method for Air Source Heat Pump: From Energetic and Economic Viewpoints." *Applied Thermal Engineering* 236: 121828.

Mumme, S., F. Brown, B. Bass, B. Shen, S. Shrestha, J. New, and K. Gluesenkamp. 2022. "Implications of Electrifying Residential Space Heating in Cold Climates with Heat Pumps, Envelope Improvements, and Thermal Storage." Conference paper. Oak Ridge, TN: Oak Ridge National Laboratory. https://www.osti.gov/biblio/1885299.

NEEP (Northeast Energy Efficiency Partnerships). (2022). "Heat pump rating representativeness study: Phase II [Report]." https://neep.org/sites/default/files/media-files/neep_heatpump_rating_representativeness_study-phase2_final.pdf

NLR (National Laboratory of the Rockies). 2026. "OCHRE: Object-Oriented Controllable High-Resolution Residential Energy Model." https://www.nlr.gov/grid/ochre.

Qu, M., Y. Tang, T. Zhang, Z. Li, and J. Chen. 2019. "Experimental Investigation on the Multi-Mode Heat Discharge Process of a PCM Heat Exchanger During TES-Based Reverse-Cycle Defrosting Using In-Cascade Air Source Heat Pumps." *Applied Thermal Engineering* 151: 154–62.

Shen, J., Z. Qian, Z. Xing, Y. Yu, and M. Ge. 2019. "A Review of the Defrosting Methods of Air Source Heat Pumps Using Heat Exchanger with Phase Change Material." *Energy Procedia* 160: 491–98.

U.S. Energy Information Administration (EIA). 2022. *2020 Residential Energy Consumption Survey (RECS) Public Use Microdata Files.* Washington, D.C.: U.S. Department of Energy. https://www.eia.gov/consumption/residential/data/2020/index.php?view=microdata

Wenju, H., J. Yiqiang, Q. Minglu, N. Long, Y. Yang, and D. Shiming. 2011. "An Experimental Study on the Operating Performance of a Novel Reverse-Cycle Hot Gas Defrosting Method for Air Source Heat Pumps." *Applied Thermal Engineering* 31(2): 363–69.

Wilcox, S. and W. Marion. 2008. Users Manual for TMY3 Data Sets. National Laboratory of the Rockies. NLR/TP-581-43156, https://docs.nlr.gov/docs/fy08osti/43156.pdf.

Woods, J., A. Mahvi, A. Goyal, E. Kozubal, A. Odukomaiya, and R. Jackson. 2021. "Rate Capability and Ragone Plots for Phase Change Thermal Energy Storage." *Nature Energy* 6: 295–302. https://doi.org/10.1038/s41560-021-00778-w.

Li, Z., W. Wei, W. Wang, Y. Sun, and S. Wang. 2024. "Determination of the Defrosting Duration Ratio for Defrosting Performance Evaluation of Air Source Heat Pump." https://doi.org/10.1016/j.jobe.2024.110305.

Milev, G., A. Al-Habaibeh, S. Fanshawe and F. Siena. 2023. "Investigating the effect of the defrost cycles of air-source heat pumps on their electricity demand in residential buildings. https://doi.org/10.1016/j.enbuild.2023.113656.

Northeast Energy Efficiency Partnerships (NEEP). 2024. Residential Heat Pump Efficiency Rating Representativeness Study: Phase II. https://neep.org/sites/default/files/media-files/neep_heatpump_rating_representativeness_study-phase2_final.pdf.